



DR MALLIKA ALVALA (Orcid ID : 0000-0003-3770-4725)

Article type : Research Article

Synthesis and Biological evaluation of morpholines linked coumarin-triazole hybrids as anticancer agents

Nerella Sridhar Goud^a, Venkatesh Pooladanda^b, S. Mahammad Ghouse^a, Jakkula Pranay^d, Santhosh Gatreddi^d, Insaf A. Qureshi^d, Ravi Alvala^c, Chandraiah Godugu^{b}, Mallika Alvala^{a*}*

a. Department of Medicinal Chemistry, National Institute of Pharmaceutical Education and Research (NIPER), Hyderabad 500 037, India

b. Department of Regulatory Toxicology, National Institute of Pharmaceutical Education and Research (NIPER), Hyderabad 500 037, India

c. G. Pulla reddy College of Pharmacy, Hyderabad, India

d. Department of Biotechnology & Bioinformatics, School of Life Sciences, University of Hyderabad, Hyderabad-500046, India.

*Corresponding Author:

Dr. Mallika Alvala

Department of Medicinal Chemistry,

National Institute of Pharmaceutical Education and Research (NIPER),

Hyderabad 500 037,

India

Tel: 9441117803

Email: mallikaalvala@yahoo.in

This article has been accepted for publication and undergone full peer review but has not been through the copyediting, typesetting, pagination and proofreading process, which may lead to differences between this version and the Version of Record. Please cite this article as doi: 10.1111/cbdd.13578

This article is protected by copyright. All rights reserved.

Abstract:

A series of novel morpholines linked coumarin-triazole hybrids (**6a-6v**) has been synthesized and evaluated for their anti-proliferative potential on a panel of five human cancer cell lines namely, bone (MG-63), lung (A549), breast (MDA-MB-231), colon (HCT-15) and liver (HepG2), using MTT assay. Among all, the compound **6n** {7-((1-(2,4-dichlorobenzyl)-1H-1,2,3-triazol-4-yl) methoxy)-4-((2,6-di methylmorpholino) methyl)-2H-chromen-2-one} showed significant growth inhibition against MG-63 cells with an IC_{50} value of 0.80 ± 0.22 μ M. Further, induction of apoptosis by **6n** of MG-63 cells confirmed as a result of morphological changes, the sub G1 phase arrest, increased percentage of apoptotic cells, and decrease in mitochondrial membrane potential and increase in ROS levels. The *in-vitro* Gal-1 expression in cell culture supernatant of MG-63 cells treated with compound **6n**, showed dose dependent reduction. The binding constant (K_a) of **6n** with Gal-1 was calculated from the intercept value which was observed as 3.0×10^5 M^{-1} by Fluorescence spectroscopy. Surface Plasmon Resonance (SPR) showed that **6n** binds to Gal-1 with binding constant (K_a) of $1.29E+04$ 1/Ms and equilibrium constant K_D value of $7.54E-07$ M respectively. Molecular docking studies revealed the binding interactions of **6n** with Gal-1.

Keywords: morpholines, coumarin-triazoles, Galectin-1, binding constant, apoptosis.

Introduction

Cancer is one of dreadful diseases in the world and characterized by uncontrolled cell growth (Rashid, 2012). According to World Health Organization (WHO), it is estimated to have a rise in the disease to over 13 million by 2030 (Bray, 2005). Despite, many anticancer agents are available but the drug induced toxicity, poor selectivity and tolerance, indicate the necessity to develop new potential anticancer agents.

Galectin-1 (Gal-1) a 14KDa laminin protein is considered to be a molecular target in the treatment of numerous cancers due to its fundamental role in tumour growth and in the multiple processes of metastasis, angiogenesis, apoptosis and invasion (Astorgues, 2014). The apoptosis is the critical cellular process, plays an important role in the cell growth maintenance and homeostasis. The changes in the regulation of apoptotic pathway have been indicated in numerous diseases including cancer (Hanahan, 2011). Therefore, ideology towards development of novel anticancer agents that would target Gal-1 protein and induce apoptosis will be more effective strategy in cancer treatment.

Coumarin (2H-chromen-2-one), a fused heterocyclic ring system consisting of benzene and 2-pyrone ring belongs to the family of neo flavonoids of plant secondary metabolites known for its wide variety of biological applications (Gormley, 1996; Fylaktakidou, 2004; Yuce, 2011; Manvar, 2011; Kostova, 2011; Hassan, 2016; Sashidhara, 2011; Thakur, 2015). Recently, Vishal K. Rajput *et al*, have reported a selective galactose based coumarin derived Galectin inhibitors and showed that the coumarin-arginine interactions are essential for Galectin inhibition through molecular modelling studies (Rajput, 2016).

1,2,3-triazole, a class of five membered aza-heterocycles, known to interact with different biomolecular targets [14] and found in many bioactive molecules (Kolb, 2003; Lal, 2016; Kharb, 2011; Kumar, 2014; Kadaba, 1988; Patp, 2012; Giffin, 2008; Buckle, 1983; Ma, 2014); Sheng, 2015). *Johan Tejler et al.*, have reported multivalent lactose derivatives with triazole moiety for selective Gal-1 inhibition (Tejler, 2006). Ring systems such as morpholine, dimethyl morpholine, piperidine, piperazine *etc.* are reported to exhibit significant cytotoxicity against various cancer cells when incorporated (Taylor, 2014).

1,2,3-Triazole linked (arylamidomethyl)-dihydrofurocoumarin hybrids **I** as phosphodiesterase inhibitors, have been reported by *A.V. Lipeeva et al.* for selective cytotoxicity (Lipeeva, 2015). Linking of coumarin with triazoles has been known for selective cytotoxicity such as Triazoles linked with 6- hydroxycoumarin **II**, chalcone-coumarin hybrid with a triazole linker **III** and Coumarin-1,2,3-triazole-dithiocarbamate hybrid **IV** against a panel of cancer cell lines [(Shakeel, 2014; Pingaew, 2014; Ye, 2014)] (**Figure 1**).

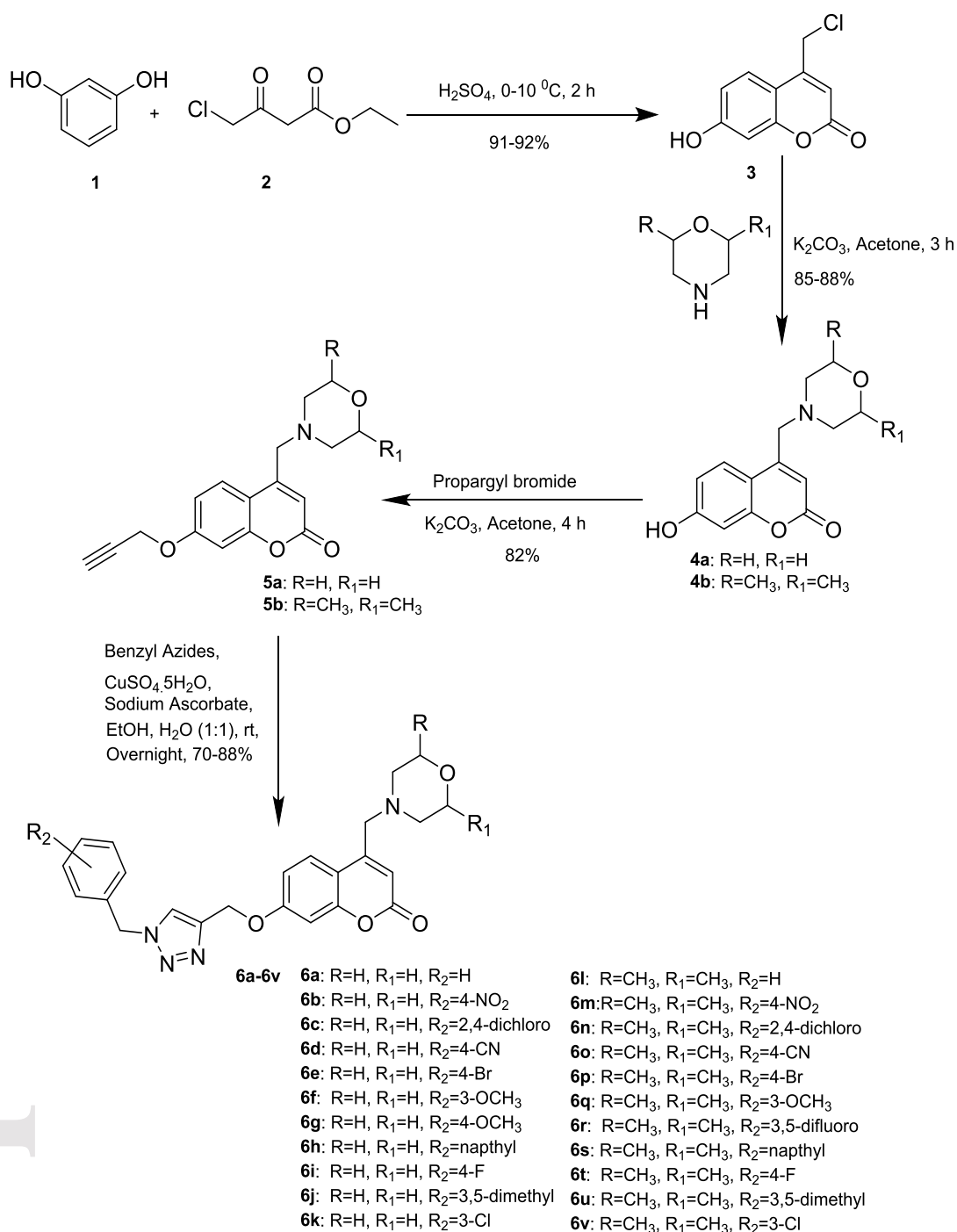
Guided by these literature investigations, and in our continuous interest to develop potent cytotoxic molecules, we have synthesized a series of morpholines linked coumarin-triazole hybrids and evaluated for their *in vitro* cytotoxicity against a panel of cancer cells are discussed herein.

Results and Discussion

Chemistry

The target compounds 7-((1-substitutedbenzyl-1H-1,2,3-triazol-4-yl) methoxy)-4-(substituted morpholino methyl)-2H chromen-2-one derivatives (**6a-6v**) were synthesized by utilizing Huisgen 1,3-dipolar cycloaddition reaction of terminal alkyne of coumarin linked morpholines (**5a, 5b**) with various benzyl azides in the presence of copper(I)-catalyst (Wang, 2017) (**Scheme 1**). Initially, the 4-(Chloromethyl)-7-hydroxy-2H-chromen-2-one (**3**) was prepared by Pechmann condensation of resorcinol (**1**) with ethyl-4-chloroacetate (**2**) in the presence of sulphuric acid (Benci, 2012). Further, Compound (**3**) was treated with substituted morpholines derivatives and offered morpholines linked coumarin intermediates **4a** and **4b**, which are further involved in the O-alkylation process with propargyl bromide in the presence of Potassium carbonate resulted morpholines linked coumarin with terminal alkyne derivatives **5a** and **5b** (Khachatryan, 2015). Finally, copper(I)-catalyzed 1,3-dipolar cycloaddition of morpholines linked coumarin with terminal alkyne derivatives (**5a, 5b**) and various benzyl azides furnished the target compounds **6a-6v** with moderate to good yields.

All synthesized compounds (**6a-6v**) were characterized by spectral techniques viz. ¹H-NMR, ¹³C NMR and HRMS. The ¹H NMR spectrum of **6a** showed characteristic protons of O- and N-attached methylene groups of morpholine ring at δ 3.60 and 2.45 ppm respectively. All the remaining protons appeared in the range of δ 3.70-8.50 ppm. ¹³C NMR spectrum showed the characteristic carbonyl and N-attached methylene carbons of morpholine at δ 161.3 and δ 53.3 ppm respectively, and all the remaining carbons appeared in the range of δ 53.7-160.7. The similar pattern was observed for rest of the compounds (**6a-6v**).



Scheme 1: Synthesis of morpholines linked coumarin-triazole hybrids (**6a-6v**).

Biological evaluation

In vitro anti proliferative activity

All the synthesized morpholines linked coumarin-triazole derivatives (**6a-6v**) were screened for their *in vitro* cytotoxicity against a panel of selected human cancer cell lines *viz.* bone (MG-63), lung (A549), breast (MDA-MB-231), colon (HCT-15) and liver (HepG2) and normal embryonic fibroblast cells (NIH-3T3) using 3-(4,5-dimethylthiazol-2-yl)-2,5-diphenyltetrazolium bromide (MTT) assay (Sharma, 2015). The IC₅₀ (μM) values of compounds **6a-6v** along with standard, Cisplatin are displayed in **Table-1**. Among the all the

derivatives, the compound **6n** has displayed significant cell cytotoxicity with an IC₅₀ value of 0.80 ± 0.22 μM, 2.97 ± 0.04 μM, 4.05 ± 2.28 μM, 3.93 ± 2.56 μM and 7.19 ± 1.12 μM against MG-63, A549, HCT-15, MDA-MB-231 and HepG2 cell lines respectively and no cytotoxicity against NIH-3T3 normal fibroblast cells. The compounds **6e**, **6i**, **6l**, **6p** and **6u** have displayed moderate cytotoxicity with IC₅₀ values in the range of 1.0 to 10 μM.

In Structural activity relationship (SAR), the coumarin scaffold with morpholines and triazole ring (**6a-6j**), attached with benzyl group bearing an electron-withdrawing groups especially halogens exhibited good cytotoxic activity in compounds viz. **6e** (R2= 4-Br), **6i** (R2= 4-F) and **6k** (R2= 3-Cl). The presence of an electron-releasing group in **6f** (3- OCH₃), **6g** (4-OCH₃) and **6j** (3,5-di CH₃) showed moderate to less cytotoxicity. In contrast, other electron-withdrawing groups in **6b** (4-NO₂), **6c** (-2,4 dichloro), **6d** (4-CN) and unsubstituted derivatives **6a** and **6h** exhibited less to no cytotoxicity. The coumarin scaffold with dimethyl morpholines and triazole ring (**6k-6v**), attached with benzyl group bearing an electron-withdrawing groups like halogens displayed significant cytotoxic activity in compounds viz. **6n** (R2= 2,4-dichloro) and **6p** (R2= 4- Br). The presence of an electron-releasing group in **6q** (3-OCH₃) and **6u** (3,5-di CH₃) showed less to good cytotoxicity.

Whereas unsubstituted derivative **6l** showed moderate activity as compared to **6s**. In contrast, other electron-withdrawing groups in **6m** (4-NO₂), **6o** (4-CN), **6r** (3,5-Difluoro), **6s** (4-F) and **6v** (3-Cl) exhibited less to no cytotoxicity. Hence, we concluded that dimethylmorpholine derivatives with an electron-withdrawing group viz. **6n** and **6p** are more cytotoxic than simple morpholine derivatives like **6e**, **6i** and **6k**.

Apoptosis studies

Morphological observations using phase contrast microscopy

Apoptosis or programmed cell death is recognized by distinctive pattern of morphological, biochemical and molecular changes occurring in a cell (Kalle, 2010). Compound **6n** treated cells (0.5, 1 and 2.5 μM) showed prominent morphological changes like cell shrinkage with rounding of cells and formation of membrane blebs as evidenced by phase contrast microscopy studies and proportional to the concentration (**Figure 2**). However, these distinctive morphological features are absent in the controlled cells.

Acridine orange/ethidium bromide (AO/EB) staining

Acridine orange/ethidium bromide (AO/EB) staining assay was used to differentiate live, apoptotic and necrotic cells (Sharma, 2016). AO/EB staining method recognize the live cells from dead cells, since AO can permeate the intact cell membrane and stain the nuclei green, whereas EB can only stain the nucleus of cells that have lost membrane integrity in orange. It can be inferred from **Figure 3** that the control cells displayed normal morphology and appeared in green colour. Fluorescence microscopic images of MG-63 cells treated with 0.5 μM concentration of compound **6n** clearly showed early stage apoptosis. The clear morphological changes such as cell shrinkage, membrane blebbing, chromatin condensation and apoptotic body formation were observed at 1 μM and 2.5 μM respectively, hence these results suggesting that **6n** induced apoptosis in MG-63 cancer cells in a dose dependent manner.

DAPI nucleic acid staining

DAPI (4',6-diamidino-2-phenylindole), a blue fluorescent dye aids in the visualization of chromatin condensation or nuclear damage and distinguishes live cells from apoptotic cells by staining the condensed nuclei of apoptotic cells was considered of interest to detect the induction of apoptosis by **6n** in MG-63 cells (Tarnowski, 1991). The results from **Figure 4** demonstrated that the nuclear structure of untreated cells was intact, whereas cells treated with **6n** displayed condensed, horse-shoe shaped or fragmented nuclei in cells.

Cell cycle analysis

Further to understand the mechanism of inhibition of cell proliferation of MG-63 cells by **6n**, cell death was quantified in terms of percentage of apoptotic cells using FACS Verse TM flow analyser (Ravi, 2011). Propidium iodide staining of cells treated with **6n** at different concentrations showed dose dependent increase in apoptotic cells (**Figure 5**). Untreated control cells exposed to DMSO-d₆ showed 3.01% cells in sub G1 phase, whereas compound **6n** treatment resulted in increased sub G1 population to 6.38% at 0.5 μM, 7.31% at 1 μM and 12.84% at 2.5 μM concentration in 24 h. These results clearly demonstrate that **6n** induce apoptosis by sub G1 phase arrest of cell cycle.

Mitochondrial membrane potential

The loss of mitochondrial membrane potential is known to be hallmark for apoptosis (Singh, 2011). Mitochondrial depolarization occurring in the early stages of apoptosis in cells treated with **6n** was investigated by JC1 (a carbocyanine cationic dye) staining. It exhibits potential-dependent accumulation in mitochondria, indicated by a fluorescence emission shift from red to green. The enhanced ROS levels induce the loss of mitochondrial membrane potential which further activates the apoptotic signalling and leads to cell death. The polarised mitochondria show red colour due to the formation of J-aggregates, whereas the depolarised mitochondria exhibit green colour due to J-monomers. **Figure 6A** shows increase population of P2 (green) mitochondrial depolarised cells in concentration dependent manner in contrast to untreated (**Figure 6A**). The loss of mitochondrial membrane potential increased in a dose dependent manner with compound **6n** (**Figure 6B**). Thus, compound **6n** induced apoptosis by inducing the mitochondrial membrane potential loss.

AnnexinV/Propidium iodide dual staining assay

To quantify the percentage of apoptosis induced by compound **6n**, the Annexin V/Propidium iodide dual staining assay (Praveen Kumar, 2016) was carried out. The Annexin V-Alexa Flour 488/PI dual staining assay facilitates the detection of live cells (LL; AV-/PI-), early apoptotic cells (LR; AV+/PI-), late apoptotic cells (UR; AV+/PI+) and necrotic cells (UL; AV-/PI+). As shown in **Figure 7**, the compound **6n** increased the percentage of late apoptotic cells from 6.19% (control) to 21.19% at 1 μM and 27.03% at 2.5 μM respectively which clearly indicates that the compound **6n** induces apoptosis in MG-63 cells in a dose dependent manner.

Measurement of ROS levels by DCFDA

The dissipation of mitochondrial membrane potential is caused by high levels of reactive oxygen species (ROS), which further leads to cause intrinsic apoptosis. The effect of **6n** on cellular ROS levels in MG-63 cells was studied by cell permeant fluorogenic dye DCFDA (2,7-dichloro fluorescein diacetate) (Eruslanov, 2010). Treatment with **6n** for 48 h caused a significant increase of ROS in MG-63 cells in dose dependent manner (0.5, 1 and 2.5 μM) as shown in **Figure 8**.

Effect of compound **6n** on Gal-1 protein levels:

Inhibition of human Gal-1 is considered as one of the potential therapeutic approaches for the treatment of cancer, as it plays a major role in tumour development and metastasis by modulating various biological functions viz. apoptosis, angiogenesis, migration, cell immune escape (Rabinovich, 2005). Effect of **6n** on Gal-1 levels during apoptosis induction was studied using Gal-1 quantitative enzyme immunoassay. Briefly, MG-63 cells were grown in 60mm cell culture dishes, treated with **6n** for 48 h and the supernatant was collected. As Gal-1 is an extracellular secreted protein, its expression can be quantified from the cellular external environment (Wu, 2018). Equal amounts of supernatant were subjected to quantitative enzyme immunoassay as per manufacture's protocol [DGAL10, R&D Systems, USA]. The supernatant was incubated with human Gal-1 coated plates and washed to remove unbound protein. Furthermore, an enzyme linked antibody was added to the reaction, specific to human Gal-1 and incubated with substrate solution for 30 minutes before terminating the reaction with 50 μL of the stop solution. Amount of protein expression was detected with the aid of a UV-spectrophotometer. Compound **6n** effectively reduced the levels of Gal-1 protein in dose dependent manner at the concentrations of 10, 30, 100 and 300 μM (**Figure 9, Table 2**).

Fluorescence Measurements for Gal-1 binding

The maximum emission spectra of Gal-1 was at 343 nm and there was decrease in fluorescence intensity with increasing concentration of the compound (**Figure 10A**). The plot of $\log[6n]$ versus $\log(\text{Fo}-\text{F})/\text{F}$ had given a linear relationship (**Figure 10B**) and the number of binding sites were calculated from the slope, which were found to be 1.13 and infers interaction of protein and compound in 1:1 ratio. The binding constant (K_a) was calculated from the intercept value which was observed as $3.0 \times 10^5 \text{ M}^{-1}$. The intensity of the fluorescence was quenched upon increase of ligand concentration and the bimolar quenching constant (K_q) was calculated to be $8.2 \times 10^{12} \text{ M}^{-1} \text{ s}^{-1}$ which is larger than diffusion control limit (Lakowicz, 2006) suggesting interaction of protein and ligand as well as the mode of quenching to be static.

Surface Plasmon Resonance (SPR) studies

The Gal-1/**6n** interaction was analyzed through SPR using immobilized Gal-1 (ligand, 8070 RU) and compound **6n** at various concentrations. Sensorgram was measured for each of concentration of compound **6n** (**Figure 11**) and fitted using 1:1 interaction steady state affinity model. SPR showed that **6n** binds to Gal-1 with binding constant (K_a) of $1.29\text{E}+04 \text{ 1/Ms}$ and equilibrium constant K_D value of $7.54\text{E}-07 \text{ M}$ respectively, using Biacore T200

Evaluation software version 2.0. SPR analysis has shown interaction of Gal-1/**6n**, which is in corroboration with fluorescence studies.

Molecular docking

The interactions of Gal-1 with the compound **6n** was studied using molecular docking calculations using the Glide module of Schrödinger suite 2014-3 (Schrödinger suite, 2014). The 3D crystal co-ordinates of human Gal-1 were retrieved from protein data bank (PDB ID: 4Y24). The docking results showed that the compound **6n** well accommodated inside the binding site of the Gal-1. The compound **6n** has shown three hydrogen bonding interactions with the essential residues of the binding site like Ser29, Asn33 and Arg48 additionally, the π - π stacking interactions with His44, His52 and Trp68 adds to the stability of the docked pose of compound **6n**. **Figure 12**, illustrate the interactions of compound **6n** with the binding site of Gal-1. It is notable from the interaction diagram that the coumarin and the triazole rings are making the key binding interactions with the binding site residues.

Conclusion

In summary, we have synthesized a series of novel morpholines linked coumarin-triazole hybrids (**6a-6v**) and characterized by spectral techniques viz. $^1\text{H-NMR}$, $^{13}\text{C-NMR}$ and HRMS. Initially, these compounds were evaluated for anti-proliferative activities on bone (MG-63), lung (A549), breast (MDA-MB-231), colon (HCT-15), liver (HepG2), using MTT assay. The compound **6n** {7-((1-(2,4-dichlorobenzyl)-1H-1,2,3-triazol-4-yl) methoxy)-4-((2,6-di methylmorpholino) methyl)-2H-chromen-2-one} exhibited significant growth inhibition against MG-63 cells with an IC_{50} value of $0.80 \pm 0.22 \mu\text{M}$ and no toxicity against NIH-3T3 fibroblast cells. Compound **6n** induced apoptosis confirmed by significant changes in cell morphology, growth arrest at sub G1 phase, increased percentage of apoptotic cells, decrease in mitochondrial membrane potential, increase in ROS levels and Gal-1 inhibition. Importance of di methyl substituted morpholines is confirmed by docking studies with Gal-1.

Materials and Methods

Chemistry

All the starting materials, reagents and solvents were purchased from commercial suppliers. Analytical thin layer chromatography (TLC) was performed on MERCK pre-coated silica gel 60-F254 aluminum plates. Visualization of the spots on TLC plates was achieved either by exposure to iodine vapour and UV light. All melting points were recorded on Stuart® SMP30 melting point apparatus and are uncorrected. Column chromatography was performed using silica gel (60-120 mesh) and was eluted with ethyl acetate-hexane. NMR spectra were recorded on Bruker 500 (500 MHz for $^1\text{H-NMR}$ and 125 MHz for $^{13}\text{C NMR}$) using CDCl_3 and DMSO-d_6 as solvents. Chemical shift was reported in parts per million (ppm) with respect to internal standard Tetra Methyl Silane (TMS). Coupling constants were quoted in Hertz (Hz). High Resolution Mass Spectra (HRMS) were obtained on Agilent Q-TOF-Mass Spectrometer 6540-UHD LC/HRMS operating at 70 eV using direct inlet. The Synthetic, biology procedures and spectral data of synthesized compounds were included in supporting information.

Conflicts of interest

The authors declare no conflicts of interest.

Acknowledgements

Thankful to Department of Biotechnology (DBT), Govt. of India, New Delhi, for the young investigators in cancer biology start up grant (6242-19/RGCB/PMD/DBT/MLKA/2015).

References

Astorgues-Xerri, L., Riveiro, M. E., Tijeras-Raballand, A., Serova, M., Neuzillet, C., Albert, S., Faivre, S. (2014). Unraveling galectin-1 as a novel therapeutic target for cancer. *Cancer Treatment Reviews*, 40(2), 307–319.

Benci, K., Mandić, L., Suhina, T., Sedić, M., Klobučar, M., Kraljević Pavelić, S., Mintas, M. (2012). Novel Coumarin Derivatives Containing 1,2,4-Triazole, 4,5-Dicyanoimidazole and Purine Moieties: Synthesis and Evaluation of Their Cytostatic Activity. *Molecules*, 17(9), 11010–11025.

Bray, F., & Møller, B. (2005). Predicting the future burden of cancer. *Nature Reviews Cancer*, 6, 63.

Buckle, D. R., Outred, D. J., Rockell, C. J. M., Smith, H., & Spicer, B. A. (1983). Studies on v-triazoles. 7. Antiallergic 9-oxo-1H,9H-benzopyrano[2,3-d]-v-triazoles. *Journal of Medicinal Chemistry*, 26(2), 251–254.

Eruslanov, E., & Kusmartsev, S. (2010). Identification of ROS Using Oxidized DCFDA and Flow-Cytometry. In D. Armstrong (Ed.), *Advanced Protocols in Oxidative Stress II* (Vol. 594, pp. 57–72).

Fylaktakidou, K. C., Hadjipavlou-Litina, D. J., Litinas, K. E., & Nicolaides, D. N. (2004). Natural and synthetic coumarin derivatives with anti-inflammatory/ antioxidant activities. *Current Pharmaceutical Design*, 10(30), 3813–3833.

Giffin, M. J., Heaslet, H., Brik, A., Lin, Y.-C., Cauvi, G., Wong, C.-H., Torbett, B. E. (2008). A Copper(I)-Catalyzed 1,2,3-Triazole Azide–Alkyne Click Compound Is a Potent Inhibitor of a Multidrug-Resistant HIV-1 Protease Variant. *Journal of Medicinal Chemistry*, 51(20), 6263–6270.

Gormley, N. A., Orphanides, G., Meyer, A., Cullis, P. M., & Maxwell, A. (1996). The Interaction of Coumarin Antibiotics with Fragments of the DNA Gyrase B Protein †. *Biochemistry*, 35(15), 5083–5092.

Hanahan, D., & Weinberg, R. A. (2011). Hallmarks of Cancer: The Next Generation. *Cell*, 144(5), 646–674.

Hassan, Mohd. Z., Osman, H., Ali, M. A., & Ahsan, M. J. (2016). Therapeutic potential of coumarins as antiviral agents. *European Journal of Medicinal Chemistry*, 123, 236–255.

Kadaba, P. K. (1988). Triazolines. 14. 1,2,3-Triazolines and triazoles, a new class of anticonvulsants. Drug design and structure-activity relationships. *Journal of Medicinal Chemistry*, 31(1), 196–203.

Kalle, A. M., Mallika, A., Badiger, J., Alinakhi, Talukdar, P., & Sachchidanand. (2010). Inhibition of SIRT1 by a small molecule induces apoptosis in breast cancer cells. *Biochemical and Biophysical Research Communications*, 401(1), 13–19.

Khachatryan, D. S., Razinov, A. L., Kolotaev, A. V., Belus', S. K., & Matevosyan, K. R. (2015). Alkylation of NH-, OH-, and SH-acids in the presence of potassium carbonate: 1. Functionalization of chloromethyl group of alkoxy-substituted aromatic aldehydes. *Russian Chemical Bulletin*, 64(2), 395–404.

Kharb, R., Shahar Yar, M., & C. Sharma, P. (2011). New Insights into Chemistry and Anti-Infective Potential of Triazole Scaffold. *Current Medicinal Chemistry*, 18(21), 3265–3297.

Kolb, H. C., & Sharpless, K. B. (2003). The growing impact of click chemistry on drug discovery. *Drug Discovery Today*, 8(24), 1128–1137.

Kostova, I., Bhatia, S., Grigorov, P., Balkansky, S., Parmar, V. S., Prasad, A. K., & Saso, L. (2011). Coumarins as antioxidants. *Current Medicinal Chemistry*, 18(25), 3929–3951.

Kumar, K., Pradines, B., Madamet, M., Amalvict, R., & Kumar, V. (2014). 1H-1,2,3-triazole tethered mono- and bis-ferrocenylchalcone- β -lactam conjugates: Synthesis and antimalarial evaluation. *European Journal of Medicinal Chemistry*, 86, 113–121.

Lakowicz J. R. (2006). *Principles of Fluorescence Spectroscopy*, Springer US, 3rd edition.

Lal, K., Yadav, P., & Kumar, A. (2016). Synthesis, characterization and antimicrobial activity of 4-((1-benzyl/phenyl-1H-1,2,3-triazol-4-yl) methoxy) benzaldehyde analogues. *Medicinal Chemistry Research*, 25(4), 644–652.

Lipeeva, A. V., Pokrovsky, M. A., Baev, D. S., Shakirov, M. M., Bagryanskaya, I. Y., Tolstikova, T. G., Shults, E. E. (2015). Synthesis of 1H-1,2,3-triazole linked aryl(arylamidomethyl) – dihydrofurocoumarin hybrids and analysis of their cytotoxicity. *European Journal of Medicinal Chemistry*, 100, 119–128.

Ma, L.-Y., Pang, L.-P., Wang, B., Zhang, M., Hu, B., Xue, D.-Q., Liu, H.-M. (2014). Design and synthesis of novel 1,2,3-triazole-pyrimidine hybrids as potential anticancer agents. *European Journal of Medicinal Chemistry*, 86, 368–380.

Manvar, A., Bavishi, A., Radadiya, A., Patel, J., Vora, V., Dodia, N., Shah, A. (2011). Diversity oriented design of various hydrazides and their in vitro evaluation against *Mycobacterium tuberculosis* H37Rv strains. *Bioorganic & Medicinal Chemistry Letters*, 21(16), 4728–4731.

Patpi, S. R., Pulipati, L., Yogeewari, P., Sriram, D., Jain, N., Sridhar, B., ... Kantevari, S. (2012). Design, Synthesis, and Structure–Activity Correlations of Novel Dibenzo[b , d]furan, Dibenzo[b , d]thiophene, and N -Methylcarbazole Clubbed 1,2,3-Triazoles as Potent Inhibitors of *Mycobacterium tuberculosis*. *Journal of Medicinal Chemistry*, 55(8), 3911–3922.

Pingaew, R., Saekee, A., Mandi, P., Nantasenamat, C., Prachayasittikul, S., Ruchirawat, S., & Prachayasittikul, V. (2014). Synthesis, biological evaluation and molecular docking of novel chalcone–coumarin hybrids as anticancer and antimalarial agents. *European Journal of Medicinal Chemistry*, 85, 65–76.

Praveen Kumar, C., Reddy, T. S., Mainkar, P. S., Bansal, V., Shukla, R., Chandrasekhar, S., & Hügel, H. M. (2016). Synthesis and biological evaluation of 5,10-dihydro-11 H -dibenzo[*b,e*] [1,4]diazepin-11-one structural derivatives as anti-cancer and apoptosis inducing agents. *European Journal of Medicinal Chemistry*, 108, 674–686.

Rabinovich, G. A. (2005). Galectin-1 as a potential cancer target. *British Journal of Cancer*, 92(7), 1188–1192.

Rajput, V. K., MacKinnon, A., Mandal, S., Collins, P., Blanchard, H., Leffler, H., Nilsson, U. J. (2016). A Selective Galactose–Coumarin-Derived Galectin-3 Inhibitor Demonstrates Involvement of Galectin-3-glycan Interactions in a Pulmonary Fibrosis Model. *Journal of Medicinal Chemistry*, 59(17), 8141–8147.

Rashid, M., Husain, A., & Mishra, R. (2012). Synthesis of benzimidazoles bearing oxadiazole nucleus as anticancer agents. *European Journal of Medicinal Chemistry*, 54, 855–866.

Ravi, A., Mallika, A., Sama, V., Begum, A. S., Khan, R. S., & Reddy, B. M. (2011). Antiproliferative activity and standardization of *Tecomella undulata* bark extract on K562 cells. *Journal of Ethnopharmacology*, 137(3), 1353–1359.

Sashidhara, K. V., Kumar, A., Chatterjee, M., Rao, K. B., Singh, S., Verma, A. K., & Palit, G. (2011). Discovery and synthesis of novel 3-phenylcoumarin derivatives as antidepressant agents. *Bioorganic & Medicinal Chemistry Letters*, 21(7), 1937–1941.

Schrödinger suite (2014). Schrödinger, LLC: New York.

Shakeel-u-Rehman, Masood-ur-Rahman, Tripathi, V. K., Singh, J., Ara, T., Koul, S., Kaul, A. (2014). Synthesis and biological evaluation of novel isoxazoles and triazoles linked 6-hydroxycoumarin as potent cytotoxic agents. *Bioorganic & Medicinal Chemistry Letters*, 24(17), 4243–4246.

Sharma, P., Senwar, K. R., Jeengar, M. K., Reddy, T. S., Naidu, V. G. M., Kamal, A., & Shankaraiah, N. (2015). H₂O-mediated isatin spiro-epoxide ring opening with NaCN: Synthesis of novel 3-tetrazolymethyl-3-hydroxy-oxindole hybrids and their anticancer evaluation. *European Journal of Medicinal Chemistry*, 104, 11–24.

Sharma, P., Thummuri, D., Reddy, T. S., Senwar, K. R., Naidu, V. G. M., Srinivasulu, G., Shankaraiah, N. (2016). New (E)-1-alkyl-1 H -benzo[*d*]imidazol-2-yl) methylene) indolin-2-ones: Synthesis, in vitro cytotoxicity evaluation and apoptosis inducing studies. *European Journal of Medicinal Chemistry*, 122, 584–600.

Sheng, J., Ma, N., Wang, Y., Ye, W.-C., & Zhao, B.-X. (2015). The application of click chemistry in the synthesis of agents with anticancer activity. *Drug Design, Development and Therapy*, 1585.

Singh, T., Sharma, S. D., & Katiyar, S. K. (2011). Grape Proanthocyanidins Induce Apoptosis by Loss of Mitochondrial Membrane Potential of Human Non-Small Cell Lung Cancer Cells In Vitro and In Vivo. *PLoS ONE*, 6(11), e27444.

Tarnowski, B. I., Spinale, F. G., & Nicholson, J. H. (1991). DAPI as a useful stain for nuclear quantitation. *Biotechnic & Histochemistry: Official Publication of the Biological Stain Commission*, 66(6), 297–302.

Taylor, R. D., MacCoss, M., & Lawson, A. D. G. (2014). Rings in Drugs: Miniperspective. *Journal of Medicinal Chemistry*, 57(14), 5845–5859.

Tejler, J., Tullberg, E., Frejd, T., Leffler, H., & Nilsson, U. J. (2006). Synthesis of multivalent lactose derivatives by 1,3-dipolar cycloadditions: selective galectin-1 inhibition. *Carbohydrate Research*, 341(10), 1353–1362.

Thakur, A., Singla, R., & Jaitak, V. (2015). Coumarins as anticancer agents: A review on synthetic strategies, mechanism of action and SAR studies. *European Journal of Medicinal Chemistry*, 101, 476–495.

Wang, X., Dai, Z.-C., Chen, Y.-F., Cao, L.-L., Yan, W., Li, S.-K., Ye, Y.-H. (2017). Synthesis of 1,2,3-triazole hydrazide derivatives exhibiting anti-phytopathogenic activity. *European Journal of Medicinal Chemistry*, 126, 171–182.

Wu, R., Wu, T., Wang, K., Luo, S., Chen, Z., Fan, M., Xu, X. (2018). Prognostic significance of galectin-1 expression in patients with cancer: a meta-analysis. *Cancer Cell International*, 18(1), 108.

Ye, X.-W., Zheng, Y.-C., Duan, Y.-C., Wang, M.-M., Yu, B., Ren, J.-L., Liu, H.-M. (2014). Synthesis and biological evaluation of coumarin–1,2,3-triazole–dithiocarbamate hybrids as potent LSD1 inhibitors. *Med. Chem. Commun.*, 5(5), 650–654.

Yuce, B., Danis, O., Ogan, A., Sener, G., Bulut, M., & Yarat, A. (2011). Antioxidative and Lipid Lowering Effects of 7, 8-Dihydroxy-3-(4-methylphenyl) Coumarin in Hyperlipidemic Rats. *Arzneimittelforschung*, 59(03), 129–134.

Figure 1. Representative examples structures of 1,2,3-triazole-coumarin hybrids (I-IV) and proposed structure of compounds **6a-6v**.

Figure 2. Morphological changes due to induction of apoptosis by **6n** were observed by phase-contrast microscopy. The MG-63 cells lost their characteristics of epithelial cells with increasing concentrations of **6n**

Figure 3. Effect of compound **6n** on apoptotic changes determined by AO/EB staining. The MG-63 cells were treated with compound **6n** with the concentration of 0.5, 1 and 2.5 μM . After 48 h of incubation, cells were stained by AO/EB dual staining. Images were captured at 200X magnification

Figure 4. Nuclear morphology of MG-63 cells treated with **6n**: Nuclear morphology of MG-63 cancer cells visualised after DAPI staining. cells were treated with different concentrations of **6n** compound for 48 h and stained with DAPI. The images were captured with fluorescence microscope at 200X. The arrows indicate the nuclear condensation and nuclear fragmentation

Figure 5. Cell cycle analysis: MG-63 Cells were treated with 0.5, 1 and 2.5 μM concentrations **6n** and analysed by propidium iodide (PI) staining after 24 h of incubation.

Figure 6. Flowcytometric analysis of the mitochondrial membrane potential: (A) mitochondrial membrane depolarisation of MG-63 cells treated with 0.5, 1 and 2.5 μM concentrations of **6n**. P1(red) indicates the percentage of polarised cells (live), where is P2(green) indicates the percentage of depolarised cells (dead). (B) Loss rate of the mitochondrial membrane potential represented by Graphpad Prism 6.01 software. Data represent as mean \pm SEM (n=3). **p<0.01 and ****p<0.0001 versus control.

Figure 7. Effect of compound **6n** on induction of apoptosis in MG-63 cells. After 48 h of compound **6n** (0.5, 1 and 2.5 μM) incubation, cells were stained with Annexin V/PI and analysed for apoptosis using BD c6 accuri flow cytometer. 30.74% apoptotic cells were observed at 2.5 μM concentration. The 10,000 cells from each sample were analysed by flow cytometry.

Figure 8. Measurement of ROS. (A) MG-63 cells were treated with **6n** (0.5, 1 and 2.5 μM) for 48 h and DCF fluorescent images were captured at 200X magnification. (B) Relative DCF fluorescence intensity was measured and represented as bar chart. Data represent as mean \pm SEM (n=3). *p<0.05 and **p<0.01 versus control.

Figure 9: (A) Gal-1 protein levels in MG-63 cells with or without **6n** at 10, 30, 100 and 300 μM concentration. (B) Human Gal-1 Standard Curve. (Data represent as Mean \pm SEM, ***p<0.001, **6n** vs. control

Figure 10: Fluorescence binding study of compound **6n** with the Gal-1. (A) Fluorescence spectra of Gal-1 in the increasing concentrations of ligand from 0 to 65 μM (from top to bottom) at pH 7.5. The protein was excited at 280 nm and emission spectra was collected in the range of 300–400 nm. (B) Modified Stern–Volmer plot of Gal-1 by compound **6n** used for the calculation of binding affinity.

Figure 11. Sensorgram of SPR for Gal-1 binding to compound **6n**. The y-axis represents the amount of bound analyte in terms of RU, while x-axis shows time after injection (seconds). The colored lines indicate different concentrations of compound **6n**.

Figure 12: 3D ligand interaction diagram of target compound **6n** (A) and co-crystal (TD-139) (B) with the binding domain of Gal-1: **6n** making interactions with Ser29, Asn33, Arg48, His44 and His52 residues of Gal-1(PDB ID: 4Y24).

Compound	MG-63 ^b	A549 ^c	HCT-15 ^d	MDA-MB-231 ^e	HepG2 ^f	NIH-3T3 ^g
6a	>30	>30	>30	>30	>30	-
6b	>30	>30	>30	>30	>30	-
6c	>30	>30	>30	>30	>30	-
6d	>30	>30	>30	>30	>30	-
6e	3.77 ± 0.17	7.82 ± 2.38	>30	>30	>30	-
6f	>30	>30	>30	>30	>30	-
6g	>30	>30	>30	>30	>30	-
6h	>30	>30	>30	>30	>30	-
6i	6.55 ± 1.02	7.55 ± 0.97	8.30 ± 0.51	9.00 ± 0.38	2.54 ± 0.23	-
6j	19.47 ± 1.40	11.96 ± 4.92	>30	>30	22.88 ± 2.72	-
6k	>30	>30	27.08 ± 5.07	22.97 ± 4.61	28.23 ± 1.45	-
6l	9.45 ± 1.31	4.78 ± 1.08	>30	>30	>30	-
6m	>30	>30	>30	>30	>30	-
6n	0.80 ± 0.22	2.97 ± 0.04	4.05 ± 2.28	3.93 ± 2.56	7.19 ± 1.12	49.07 ± 0.09
6o	>30	>30	>30	>30	>30	-
6p	1.72 ± 0.09	9.97 ± 3.57	>30	>30	>30	-
6q	>30	>30	>30	>30	>30	-
6r	>30	>30	>30	>30	>30	-
6s	>30	>30	>30	>30	>30	-
6t	>30	>30	>30	>30	>30	-
6u	1.89 ± 0.05	10.93 ± 0.65	>30	>30	>30	-
6v	>30	>30	19.50 ± 1.02	>30	14.25 ± 2.52	-
Cisplatin	17.42 ± 0.77	24.15 ± 2.14	19.45 ± 1.75	16.97 ± 2.45	25.73 ± 1.41	-

Table 1. IC₅₀ (μM) values^a for the derivatives **6a-6v** determined by MTT assay.

^a50% Inhibitory concentration after 48 h of drug treatment. ^b Human osteosarcoma. ^c Human lung cancer. ^d Human colon cancer. ^e Human breast cancer. ^f Human liver cancer. ^g Mouse embryonic fibroblast cells.

Table 2. Amount of Gal-1 protein in control and compound **6n** (10, 30, 100 and 300 μM) treated MG-63 cells.

Concentration	Absorbance at 450 nm	Gal-1 concentration($\mu\text{g/mL}$)
Control	0.6074	4.03
6n (10 μM)	0.6060	4.02
6n (30 μM)	0.5493	3.49
6n (100 μM)	0.4143	2.24
6n (300 μM)	0.2786	0.97

Figure 1

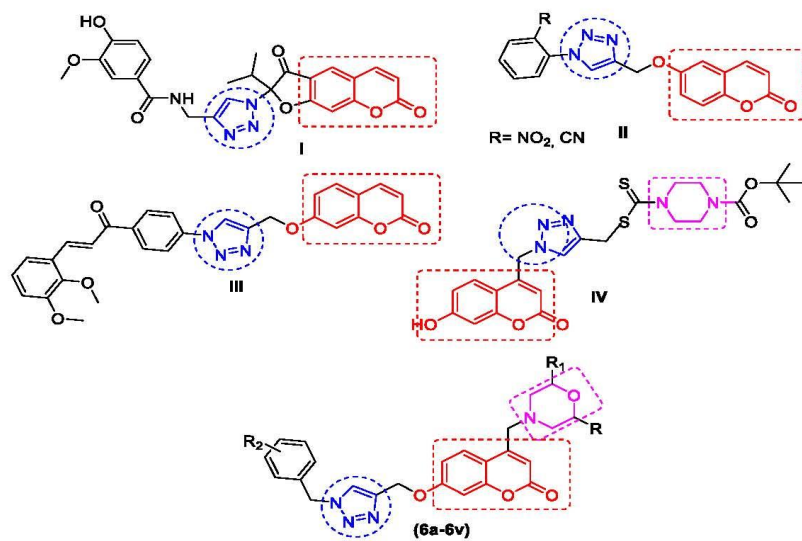


Figure2:

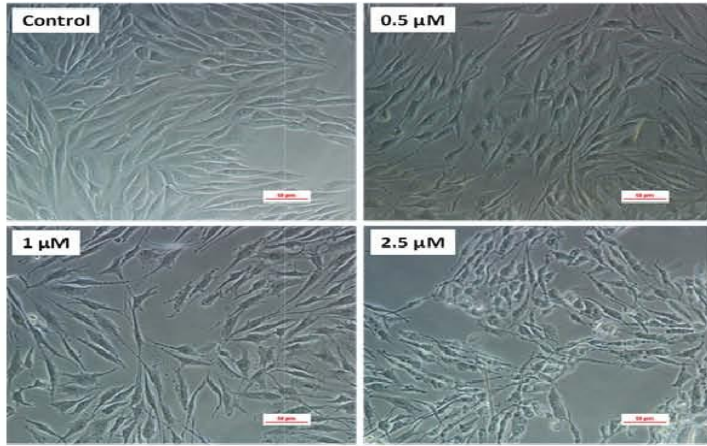


Figure3:

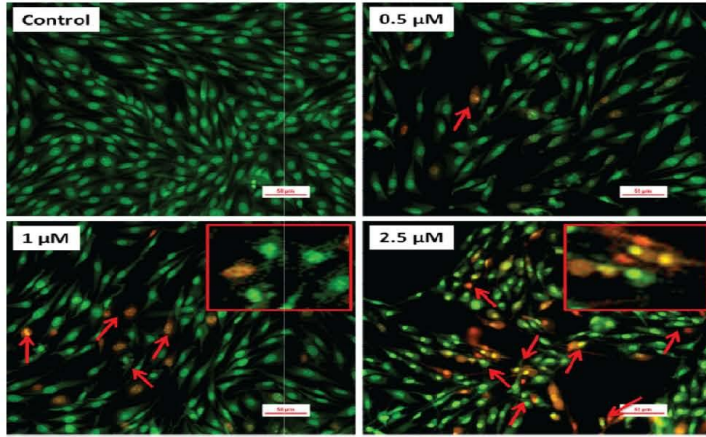


Figure4:

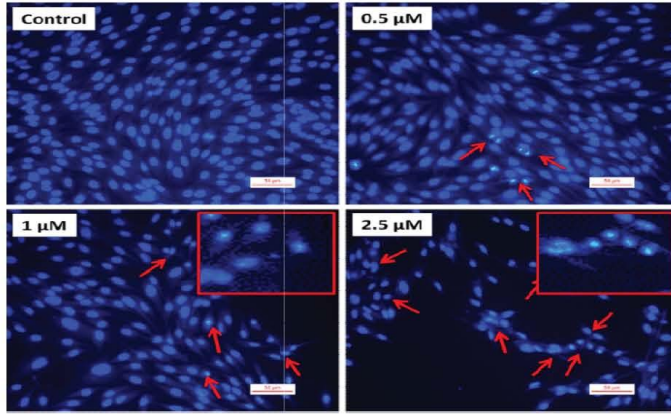


Figure5:

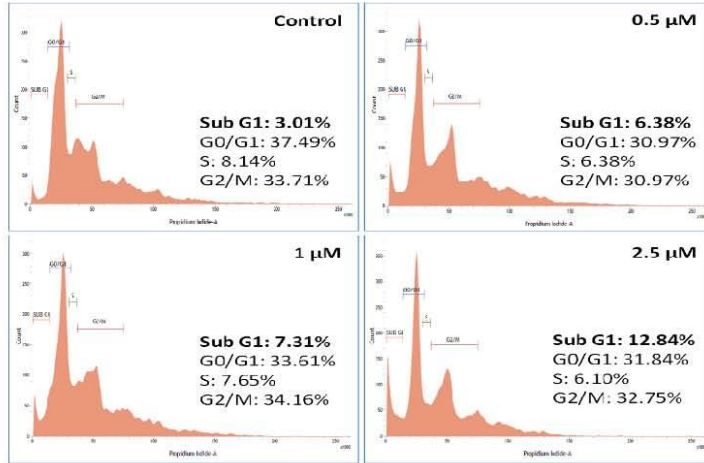


Figure6:

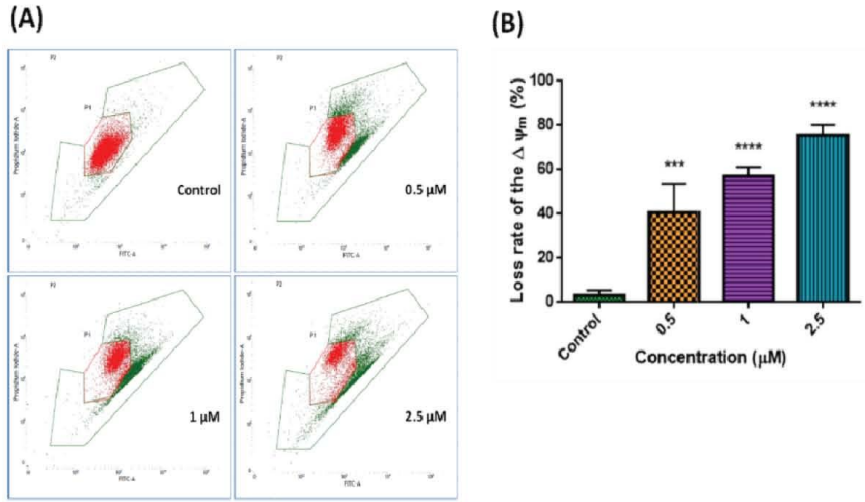


Figure7:

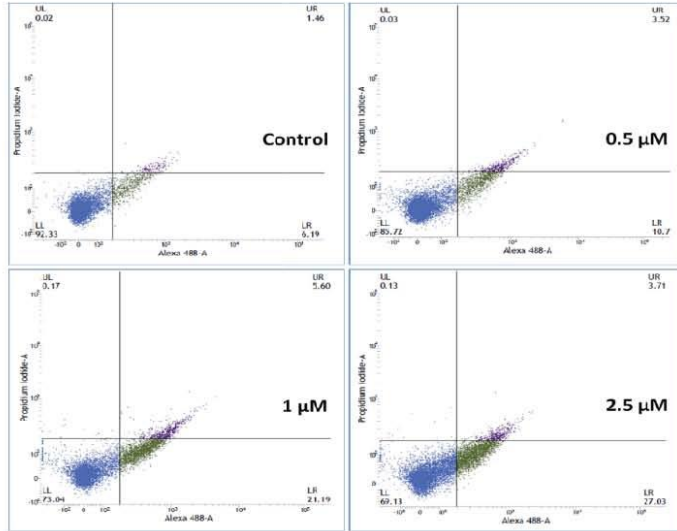


Figure8:

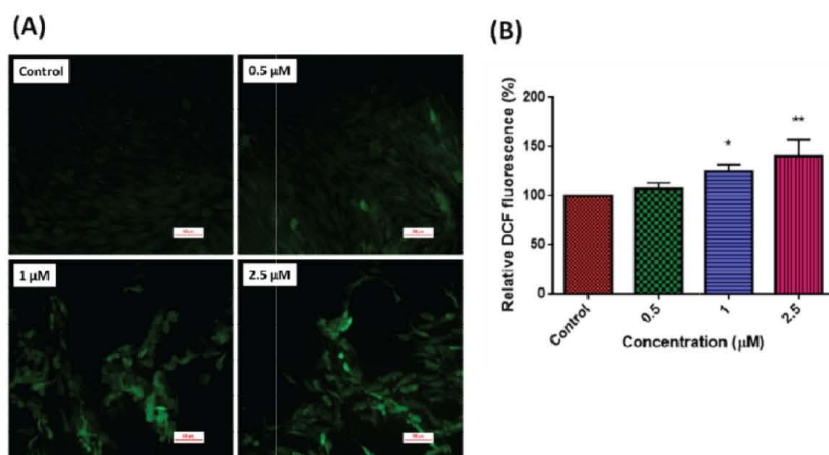


Figure9:

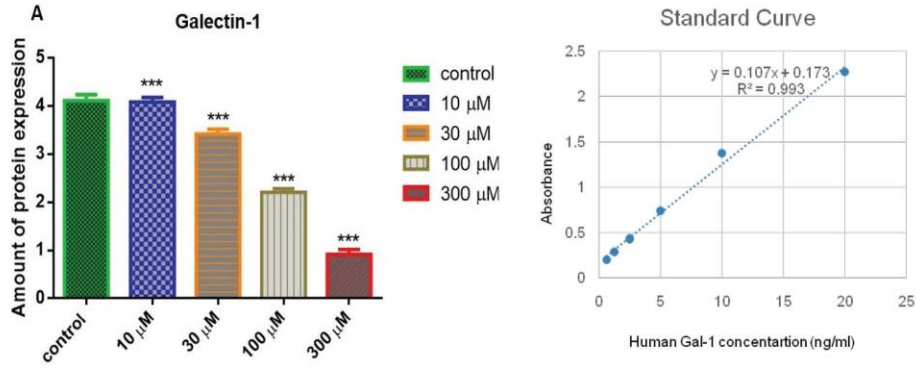


Figure10:

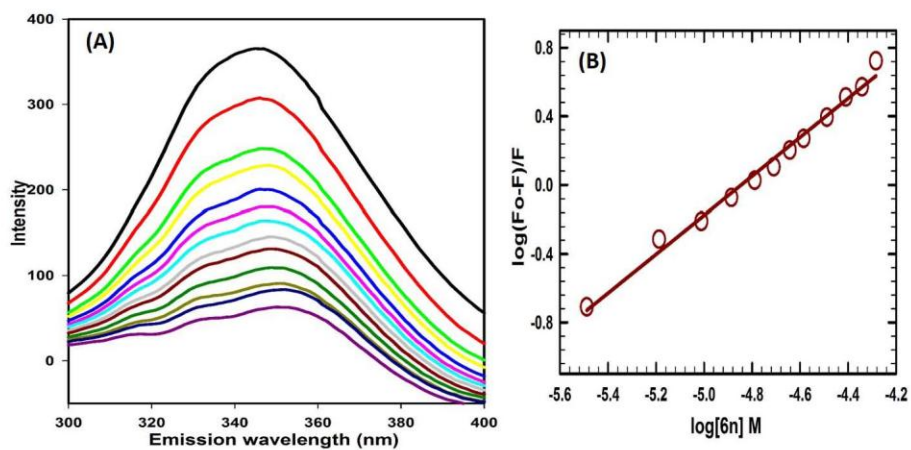


Figure11:

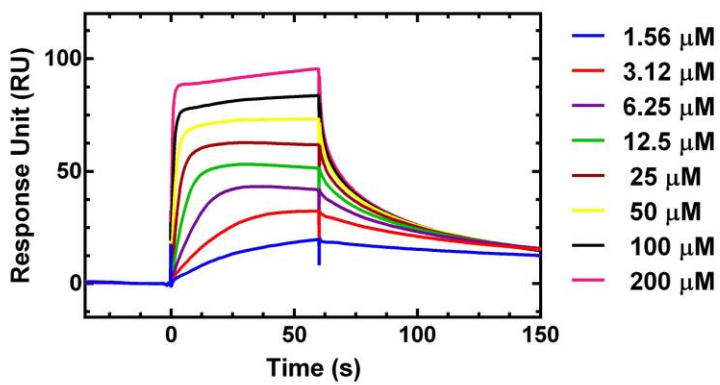


Figure12:

